Geophys. J. Int. (1993) **115**, 905–920

Late Quaternary kinematics of the Pallatanga strike–slip fault (Central Ecuador) from topographic measurements of displaced morphological features

Thierry Winter,[1] Jean-Philippe Avouac[2] and Alain Lavenu[3]

[1] *Laboratoire de Tectonique, IPGP, 4, place Jussieu, 75252 Paris, France*
[2] *Laboratoire de Détection Géophysique, CEA, 91680 Bruyères-le-Châtel, France*
[3] *ORSTOM, Dept TOA, UR 1H, 213 rue Lafayette, 75480 Paris cedex 10, France*

Accepted 1993 May 4. Received 1993 May 4; in original form 1993 January 14

SUMMARY

The northeast-trending Pallatanga right-lateral strike–slip fault runs across the Western Cordillera connecting N50°E–N70°E trending normal faults in the Gulf of Guayaquil with N–S reverse faults in the Interandean Depression. Over most of its length, the fault trace has been partly obscured by erosional processes and can be inferred in the topography only at the large scale. Only the northern fault segment, which follows the upper Rio Pangor valley at elevations above 3600 m, is prominent in the morphology. Valleys and ridges cut and offset by the fault provide an outstanding record of right-lateral cumulative fault displacement. The fault geometry and kinematics of this particular fault segment can be determined from detailed topographic levellings. The fault strikes N30°E and dips 75° to the NW. Depending on their size and nature, transverse morphological features such as tributaries of the Rio Pangor and intervening ridges, reveal right-lateral offsets which cluster around 27 ± 11 m, 41.5 ± 4 m, 590 ± 65 m and 960 ± 70 m. The slip vector deduced from the short-term offsets shows a slight reverse component with a pitch of about 11.5° SW. The 41.5 ± 4 m displacements are assumed to be coeval with the last glacial termination, yielding a mean Holocene slip-rate of 2.9–4.6 mm yr^{-1}. Assuming a uniform slip rate on the fault in the long term, the 27 m offset appears to correlate with an identified middle Holocene morphoclimatic event, and the long term offsets of 590 m and 960 m coincide with the glacial terminations at the beginning of the last two interglacial periods.

Key words: fault slip, South America, topography.

INTRODUCTION

Although instrumental and historical seismicity attest to intense active deformation (e.g. Kelleher 1972; Stauder 1975; Barazangi & Isacks 1976; Pennington 1981; Chinn & Isacks 1983; Suarez, Molnar & Burchfield 1983), the active tectonics of Ecuador remain poorly known. Active faulting in Ecuador has only recently been recognized and studied in the field (Soulas 1988; Winter & Lavenu 1989; Winter 1990; Soulas *et al.* 1991). A major feature is the right-lateral Dolores–Guayaquil Megashear (Fig. 1a), which appears to be a reactivated Mesozoic suture between accreted terranes and continental South America (Case *et al.* 1971, 1973; Campbell 1974a and b; Feininger & Bristow 1980; Feininger & Seguin 1983; McCourt, Apsden & Brook 1984; Bourgeois *et al.* 1985; Lebrat, Megard & Dupuy 1985a and b). In northern Ecuador, the Dolores–Guayaquil Megashear follows the western border of the Interandean Depression and is expressed by successive reverse faults affecting upper Miocene to Quaternary infilling of the Interandean Depression (Winter 1990) (Fig. 1b). South of latitude 2°S, it bends toward the Gulf of Guayaquil, where it merges with WSW–ENE-trending normal faults (Fig. 1b). Extensional tectonics in the Gulf of Guayaquil began in the Miocene, and is thought to be related with the onset of right-lateral strike–slip displacement along the Dolores–Guayaquil Megashear (Malfait & Dinkelman 1972; Faucher & Savoyat 1973; Campbell 1974a and b; Benitez 1986).

The 200 km long Pallatanga fault is a part of the Dolores–Guayaquil Megashear (Soulas 1988; Winter & Lavenu 1989; Winter 1990; Soulas *et al.* 1991). It follows the entrenched valley of the Rio Pangor and runs across the

Western Cordillera up to the foot of Chimborazo volcano, west of the Interandean Depression (Figs 1b and 2). It thus appears to connect N50°E–N70°E normal faults in the Gulf of Guayaquil with N–S reverse faults along the Interandean Depression (Winter 1990) (Fig. 1b).

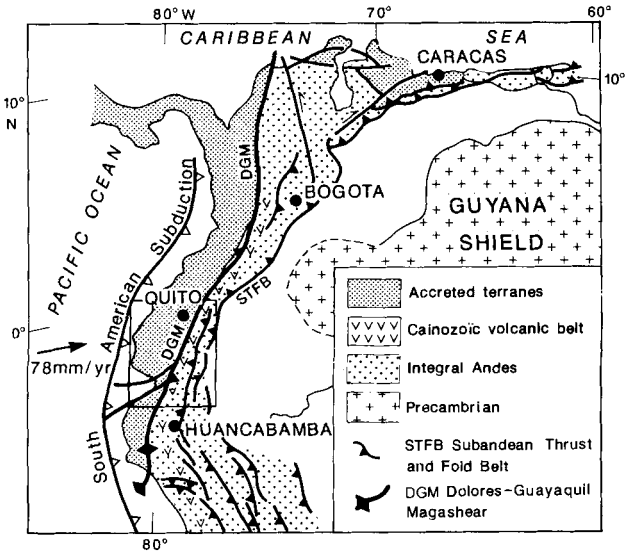

Figure 1(a). Major structural units of northwestern South America, modified from Megard (1987). Box depicts area shown in Fig. 1(b).

Because of the very humid climate, the fault trace has been obliterated by continuous hillslope processes and frequent landslides for over most of its length. Nevertheless, along the upper Rio Pangor valley, between the towns of Pallatanga and Cajabamba, where the climate is colder and drier due to the high elevation (above 3600 m), the fault trace is well preserved (Fig. 2). This is the area where Winter & Lavenu (1989) observed extensive morphological evidence for right-lateral displacements. Geomorphic features can be used to determine amount of fault displacements (e.g. Clark 1970; Sieh 1978). Interpretation of the morphology in view of the Late Quaternary climatic record can further allow for the determination of slip rates (Armijo *et al.* 1986; Peltzer *et al.* 1988).

We applied this approach to the study of the fault segment near Cajabamba. This study relies primarily on a detailed morphological and topographic survey and an interpretation of the morphology in view of the Late Quaternary regional climatic record. It allows determination of the fault geometry and kinematics.

MORPHOLOGICAL EVIDENCE FOR RIGHT LATERAL AND REVERSE SLIP ON THE PALLATANGA FAULT

The studied fault segment (box in Fig. 2) lies at the base of a steep range front which reaches elevations above 4000 m

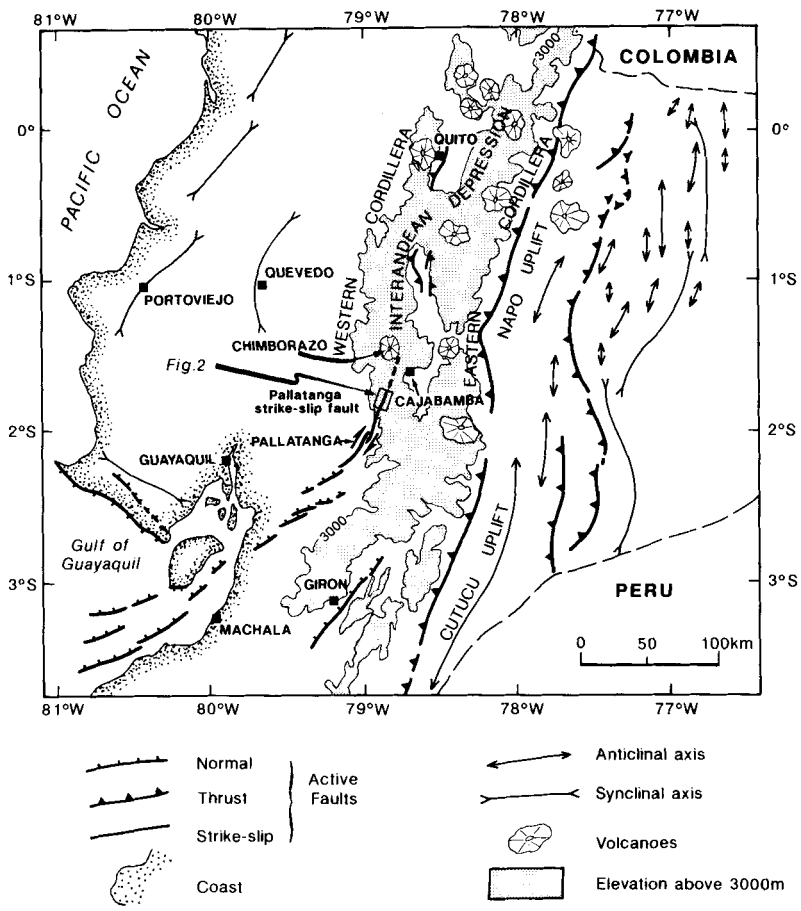

Figure 1(b). Active tectonics and topography of Central Ecuador. Active faults and folds were interpreted from 1/1,000,000 geological map of Ecuador and Landsat mosaic. Modified from Winter (1990). Box depicts area shown in Fig. 2.

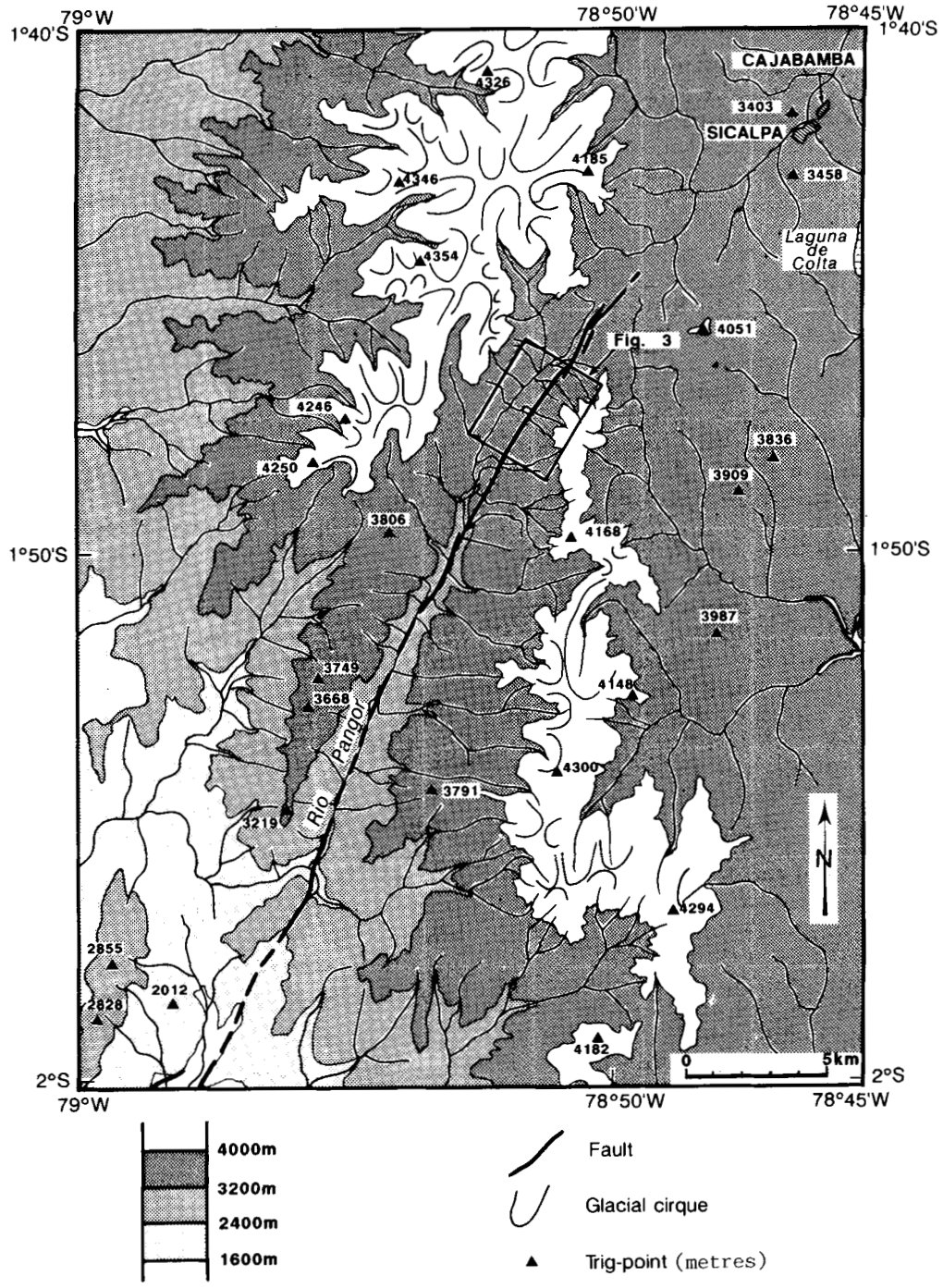

Figure 2. Topographic map of the Pallatanga fault along the Rio Pangor valley. Note extinct glacial cirques in mountains. Box depicts area shown in Fig. 3.

and which bears marks of now extinct glacial cirques. The fault runs along the eastern border of the Rio Pangor valley, up to a 3900 m high pass across the Western Cordillera. On the air photo of Fig. 3, the fault makes a sharp and straight N30°E trace cutting across the landscape. Landforms are strongly disturbed in the vicinity of the fault trace. Numerous landslides can be identified on the air photos, and many small rivers and gullies have apparently developed upstream from the fault by headward erosion from downhill-facing scarps, with some of them having probably been initiated by landslides (Figs 3a and b). In the field, the fault trace makes a clear break in slope across the foothills, suggesting general uplift of the downstream fault block (Fig. 4). In fact, fault scarps shown on Fig. 3(b) face either to the northwest or to the southeast depending on the orientation of the topography, which is characteristic of strike–slip faults (Peltzer *et al.* 1988). Free faces have been eroded away, but scarp slopes are still steep (27° to 30°), attesting to recent and sustained activity. Flat swampy depositional areas have systematically formed at places where the

drainage has been dammed by uphill-facing fault scarps (Fig. 5). The presence of these swampy areas bounding the fault trace, even where the topography close to fault trace is horizontal, also attests to general uplift of the downstream fault block. The range front itself cannot, therefore, be considered as the long-term expression of the fault displacement. It probably has been exhumed by river entrenchment localized along the fault, because brecciated materials in the fault zone should be particularly erodible.

The fault cuts across tributaries of the Rio Pangor. These tributaries have entrenched into alluvium of the Rio Pangor, probably as a response to entrenchment of the Rio Pangor itself, and have thus formed a contrasted topography of valleys and ridges. On the aerial view (Fig. 3a) it can be seen that most of these valleys and ridges are deviated right laterally across the fault zone. All deviations are not the same however. It seems that the rivers have responded differently to the perturbation of their geometry by fault movement, probably according to their size and erosional power (see Gaudemer, Tapponnier & Turcotte 1990, for a general discussion of this phenomenon). At the small scale, the rills and gullies that cross the fault indicate variable right-lateral offsets up to a few metres. Highly variable offsets are mostly observed where flat swampy depositional areas have formed. The major rivers, notated V_i in Fig. 3(b), appear to have recorded larger offsets than small secondary tributaries. The clearest example may be that of the Quebrada Pulala which is sharply offset by about 37 m (Figs 3 and 6). Several intervening ridges a few metres high, with a typical width of about 50 m, are clearly cut by the fault and consistently offset by a few tens of metres (Fig. 7).

The fault trace appears to mark a morphological discontinuity at a large scale as well. Some large valleys and ridges with a characteristic width of a few hundred metres seem to abut abruptly against the fault. Such is the case for the now abandoned valleys V_4' and V_5', in the downstream fault-block, which both face crest CR_2 in the upstream fault block. The sizes of these valleys appear too large when compared to their relatively small present catchment area. We, therefore, suggest that these large valleys formed at a time when they drained large valley catchments in the upstream fault block, which have been subsequently offset by the fault. The discontinuity across the fault zone of these major crests and valleys would indicate long-term fault displacements of the order of a few hundred metres.

QUANTITATIVE ANALYSIS

Methodology

In order to determine fault-plane geometry and short- and long-term offsets, an aerial photo interpretation has been coupled with detailed topographic levellings. In their study of the Chang Ma fault (Gansu, China), Peltzer *et al.* (1988) proposed that cumulative lateral offsets can be measured by correlating topographic profiles levelled parallel to the fault trace on either side of the fault. They observed that size of offsets depends on the characteristic size of the topographic features correlated. Large valleys and ridges, with a typical width of a few hundred metres, showed offsets clustering around 500 m, whereas narrower valleys and ridges, with a typical width of a few tens of metres, were offset by about 50 m. Because of their different wavelength, the two sets of topographic features could be easily extracted by filtering of the profiles. This study confirmed that the genesis and evolution of the morphology is not a continuous process, but rather a process punctuated by large morphogenetic episodes, possibly correlated with glacial pulses. Peltzer *et al.* (1988), moreover, suggested that the two sets of topographic features were inherited from the two last glacial terminations, a scenario consistent with a constant strike–slip rate on the fault.

Our observations lead us to a slight modification of the procedure proposed by Peltzer *et al.* (1988). Close to the fault, the morphology has been submitted to frequent and significant reshaping so that evidence for only short-term offsets is clearly preserved. Away from the fault, landforms are more stable, and longer term offsets may be better documented. Rather than filtering different wavelengths on a unique pair of profiles, we preferred an analysis relying on several sets of profiles levelled at various distances from the fault. This method allows, moreover, systematic azimuthal correction for the obliquity of the structures relative to the fault strike.

We opted for three pairs of profiles levelled parallel to the fault on each side of the fault trace. The first pair, P_u–P_d, followed the top and the base of the fault scarp itself, thus bounding the fault trace upwards and downwards. The second set, P_{-40}–P_{60} was run about 40 m downstream and 60 m upstream (in order to avoid upstream extension of flat swampy depositional areas) from the fault trace, and the third set, P_{200}–P_{-200}, was about 200 m away from the fault trace. These profiles are located on Fig. 8. We used the same total station (theodolite coupled with an infrared distance meter) as Peltzer *et al.* (1988). Points were recorded by their geographic coordinates, according to a unique reference origin.

Determination of the fault geometry

The fault plane geometry can be determined from the fault trace, which, by definition, marks the intersection of the fault plane with the topographic surface. The profiles run at the base and the top of the fault scarp were projected on various vertical planes with various azimuths. We sought the direction that best projects the profiles on a single straight line within that plane. This configuration is obtained for a vertical plane of projection perpendicular to the fault azimuth. We obtained a well-constrained fault plane striking N30°E and dipping 75° to the west (Fig. 9).

Short-term offsets

The clearest short-term displacements were found along the northern fault segment (Fig. 10). There, several ridges with a characteristic spacing of about 150 m are cut by the fault and right-laterally offset by a few tens of metres (cr_1, cr_2 and cr_3 in Fig. 10). Fig. 11 is a detailed map of this site which was drawn on the basis of our topographic measurements. Profiles P_u and P_d have been projected in a plane striking parallel to the fault trace (Fig. 12a). Because of the right-lateral displacement of the non-horizontal topography, the fault scarp faces to the southeast (upstream) where the fault cuts across a topography sloping to the northeast, and

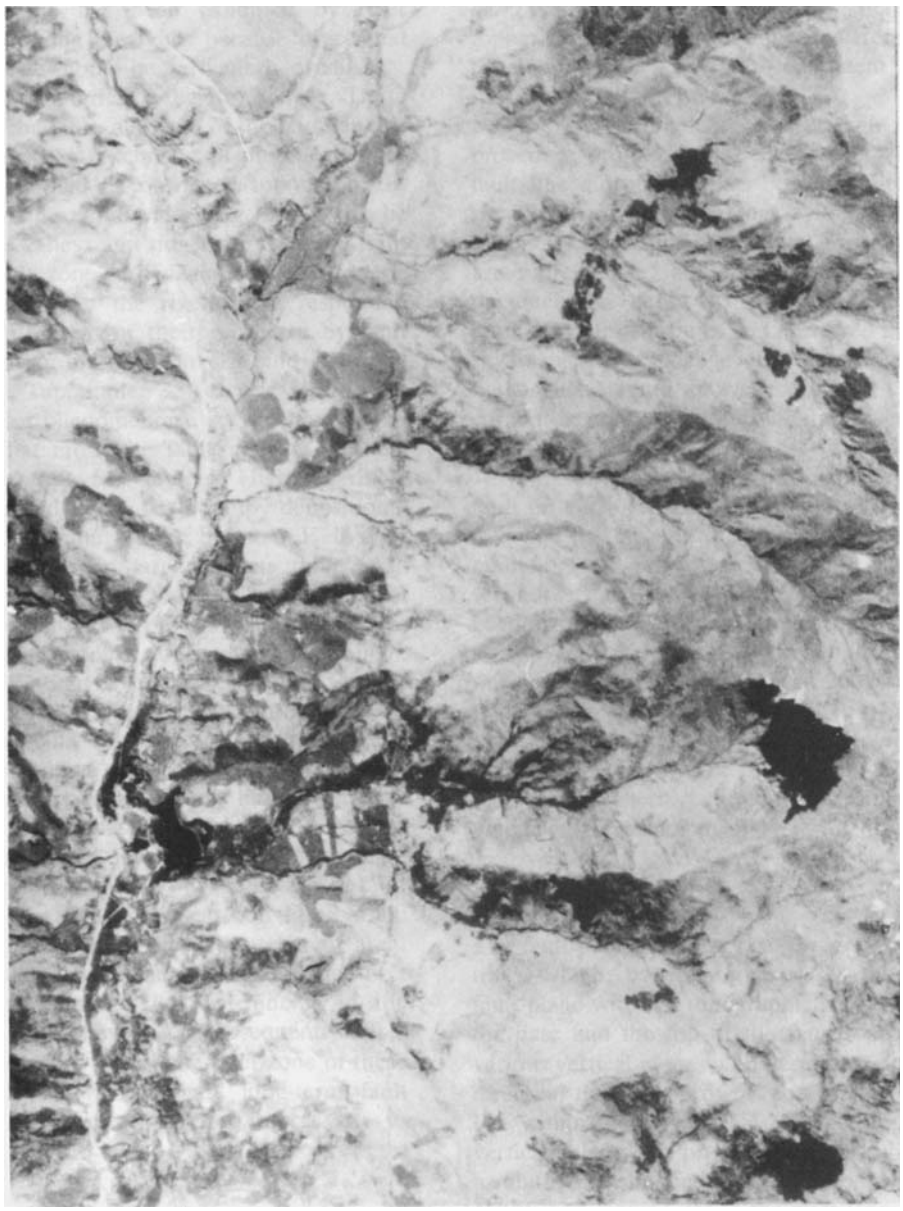

(a)

Figure 3. (a) Aerial view of the studied area. See box in Fig. 2 for location. (b) Morphotectonic interpretation of (a). Note the sharp and linear fault trace across the morphology.

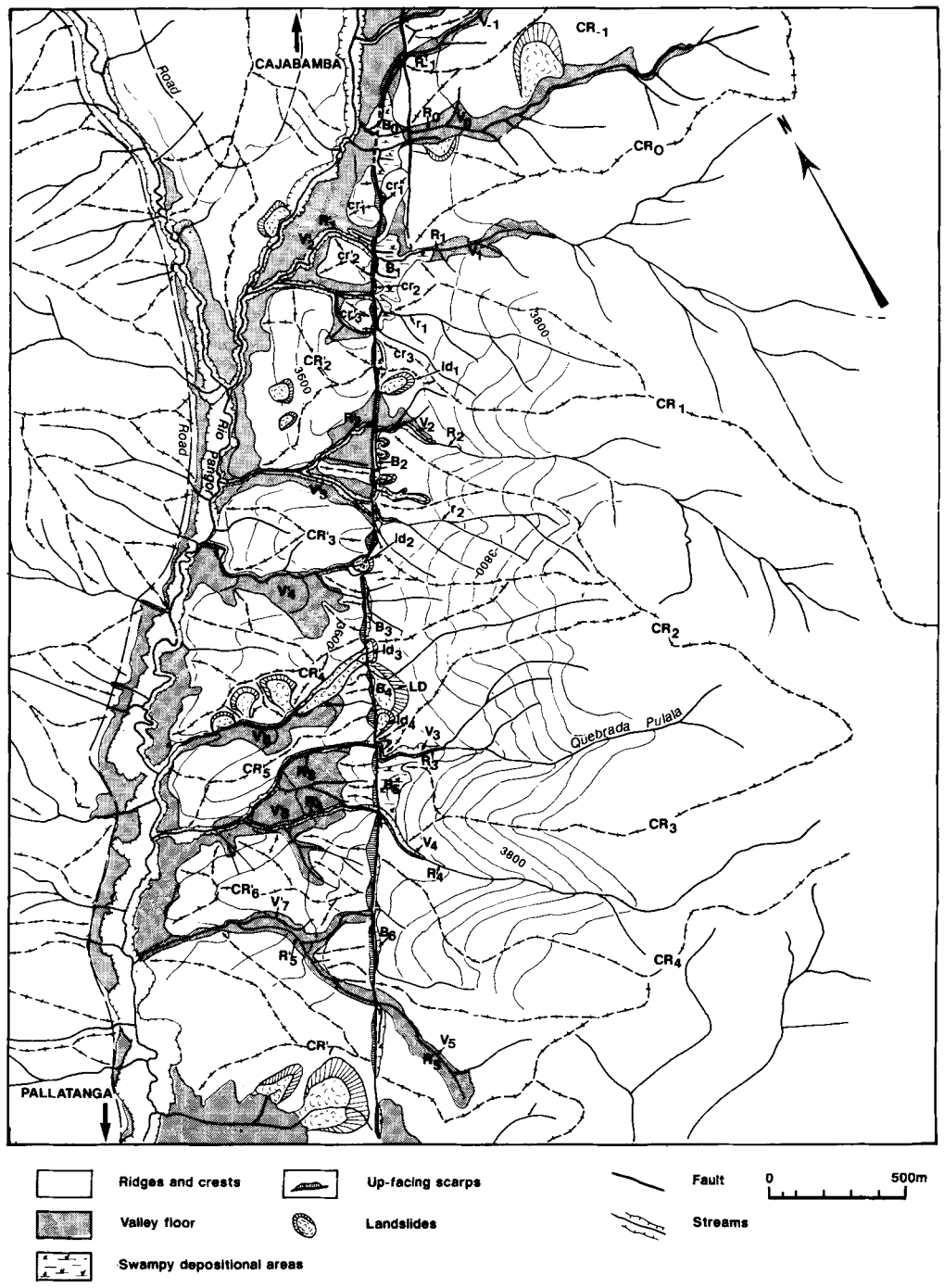

(b)

Figure 3. (*Continued.*)

faces to the northwest (downstream), where the topography slopes to the southwest. Crests cr_1–cr_1', cr_2–cr_2', cr_3–cr_3' and rivers R_1–R_1' and r_1–r_1' indicate right-lateral offsets that can be measured on this projection. Given that P_u and P_d are only a few metres apart and that most features are nearly perpendicular to the fault strike (Fig. 11), azimuthal corrections can be neglected. Offsets between 4 m and 27 m are measured (Fig. 12a). These offsets differ because the morphological features probably have different ages or because they have been eroded differently. For example, crests cr_2 and cr_3, formed as a result of river entrenchment in highly erodible and swampy deposits dammed by the fault scarp, probably are intensely reshaped by erosion. Crest cr_1–cr_1' has been better preserved, and an apparent slip vector S_0, with a vertical component of 5.2 m and a horizontal component of 27 m, can be measured (Fig. 12, inset). The uncertainty of such a measurement is difficult to quantify. Measurement errors on levelled points (of the order of a few centimetres at most) are negligible compared to the topographic irregularities due to the topographic

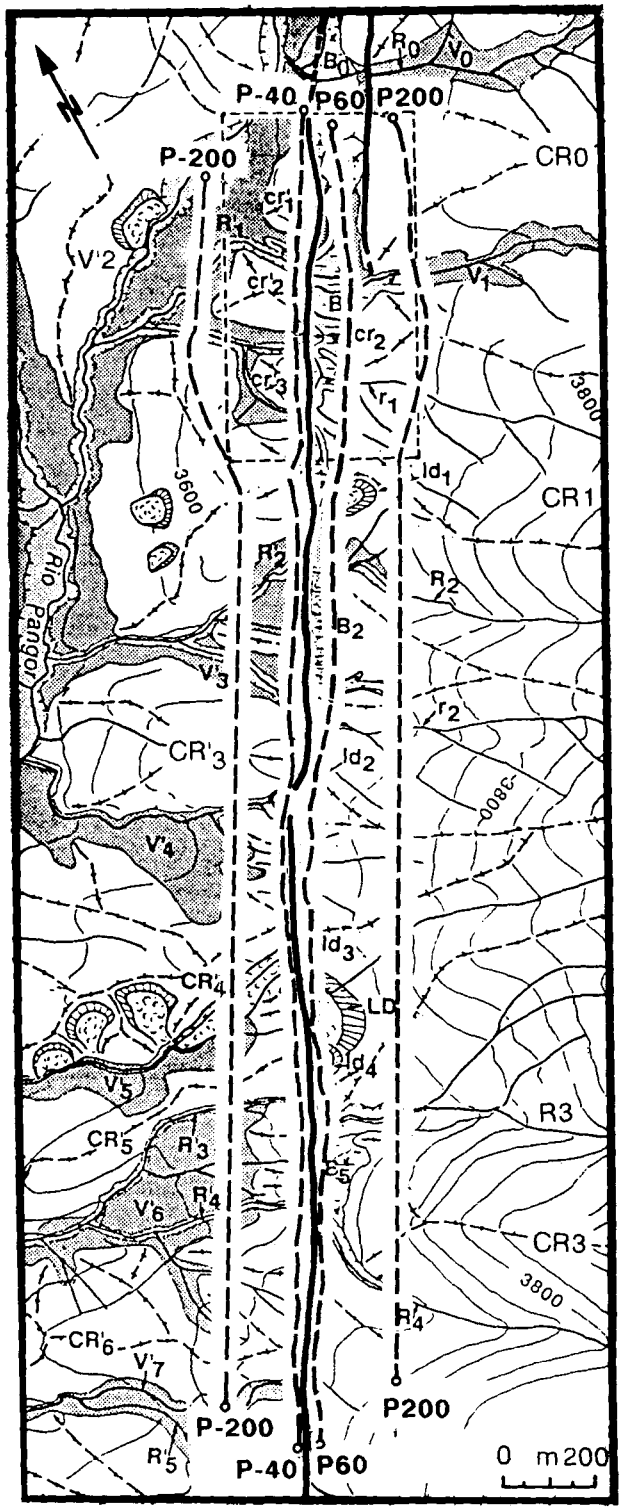

Figure 8. Location of profiles levelled in the field. Profiles are named according to their location: for instance, *P*-200 was levelled parallel to and 200 m downstream from the fault trace.

natural roughness. A major source of uncertainty arises because, once offset, a morphological feature can be modified by surface processes so that a perfectly continuous morphological feature at the fault trace can not generally be restored. Considering either the northeastern or the southwestern flank of crest cr_1–cr'_1, we estimate that the horizontal and the vertical offset might be in error of at most 11 m and 1 m, respectively. This yields for S_0 a strike–slip component of 27 ± 11 m, and a vertical component of 5.2 ± 1.0 m. Here, the error bars should be considered as ranges, i.e. 100 per cent confidence interval. A shift of the whole profile according to the slip vector S_0 also puts cr_2 and cr'_2 in rough correlation (Fig. 12b). This configuration suggests that rivulet R_1 previously flowed in R'_1, and that r_0, which is now facing R'_1, must have developed recently by regressive headward spring erosion. By contrast r_1 is apparently not offset at the fault trace. In map view, a cumulative offset of a few tens of metres is, however, obvious (Fig. 11). It seems that river r'_1, at the same time it was offset by the fault, has entrenched laterally in the downstream fault block, whereas its previous channel, upstream from the fault, has been filled with sediments. The river has thus been able to maintain a relatively continuous course across the fault.

Crest cr_1–cr'_1 has a sigmoidal shape in map view (Figs 11 and 13), suggesting that it has recorded a cumulative fault displacement larger than the net 27 m offset measured at the fault trace. A profile levelled along the top of the crest outlines the deflection of the crest near the fault. A few metres away from the fault, the crest is nearly linear so that it can be extrapolated linearly onto the fault trace with some confidence (Fig. 13). A total offset of about 40 m is then obtained, which accounts for the net 27 m offset at the fault trace and the deflection of the crest. Our interpretation is that the ridge has been offset by about 40 m since the time it was first carved as a ridge across the fault, but when it had been offset by about 13 metres, it was reshaped by intense erosional processes, that totally smoothed out the ridge discontinuity at a time (inset in Fig. 13).

If the map of Fig. 11 is cut along the fault trace and if a 40 m right-lateral fault displacement is restored (Fig. 14), the morphologic and topographic discontinuities across the fault trace are almost entirely smoothed out. This configuration restores the crests cr_2–cr'_2, cr_3–cr'_3 and the rivers R_1–R'_1 and r_1–r'_1 as continuous features. All these morphological features thus appear to have recorded, like crest cr_1–cr'_1 a 27 m offset, since the last reshaping episode and a 40 m total offset since they first formed across the fault trace.

The profile levelled along the top of the crest cr_1–cr'_1 and another profile levelled along the valley floor R_1–R'_1 (see location in Fig. 11) have been projected on a vertical plane striking perpendicularly to the fault trace in Fig. 9. Restoring crest cr_1–cr'_1 to a continuous feature implies that it has experienced a vertical cumulative displacement of about 8 metres, apparently larger than the 5.2 ± 1 m determined at the fault trace. This displacement would also restore a satisfactory continuous profile for the valley floor R_1–R'_1, if the shaded area in Fig. 9 is assumed to represent sedimentation against the fault scarp. Vertical displacements between 6 m and 9 m would actually be admissible. The slip vector, S1, corresponding the total offset of crest cr_1–cr'_1 has a strike–slip component of about 40 m and a vertical component of about 8 m. The pitch of the short-term offsets S_1 and S_0, related to the crest cr_1–cr'_1, resolved on the fault plane appear to be similar. They yield the same reverse right-lateral pitch of about 11–12°SW.

Profiles P_{60}, on the eastern block, and P_{-40}, on the

Figure 4. South-looking view of the studied fault segment. Arrows point to the fault trace. Note the discontinuity of the ridges and valleys across the fault trace.

(a)

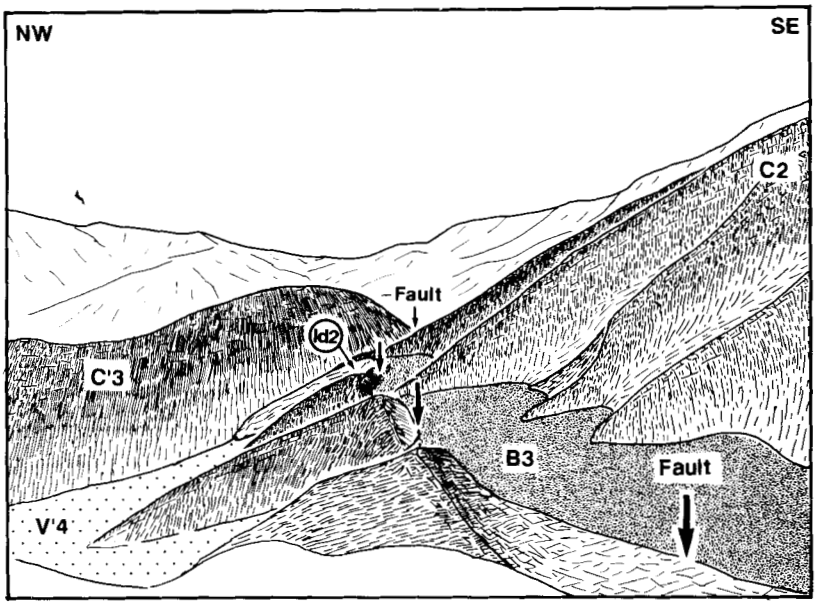

(b)

Figure 5. (a) North-looking view of the fault trace where a flat swampy depositional area (B3) has formed against an upward-facing fault scarp. (b) Sketch of photograph 5(a).

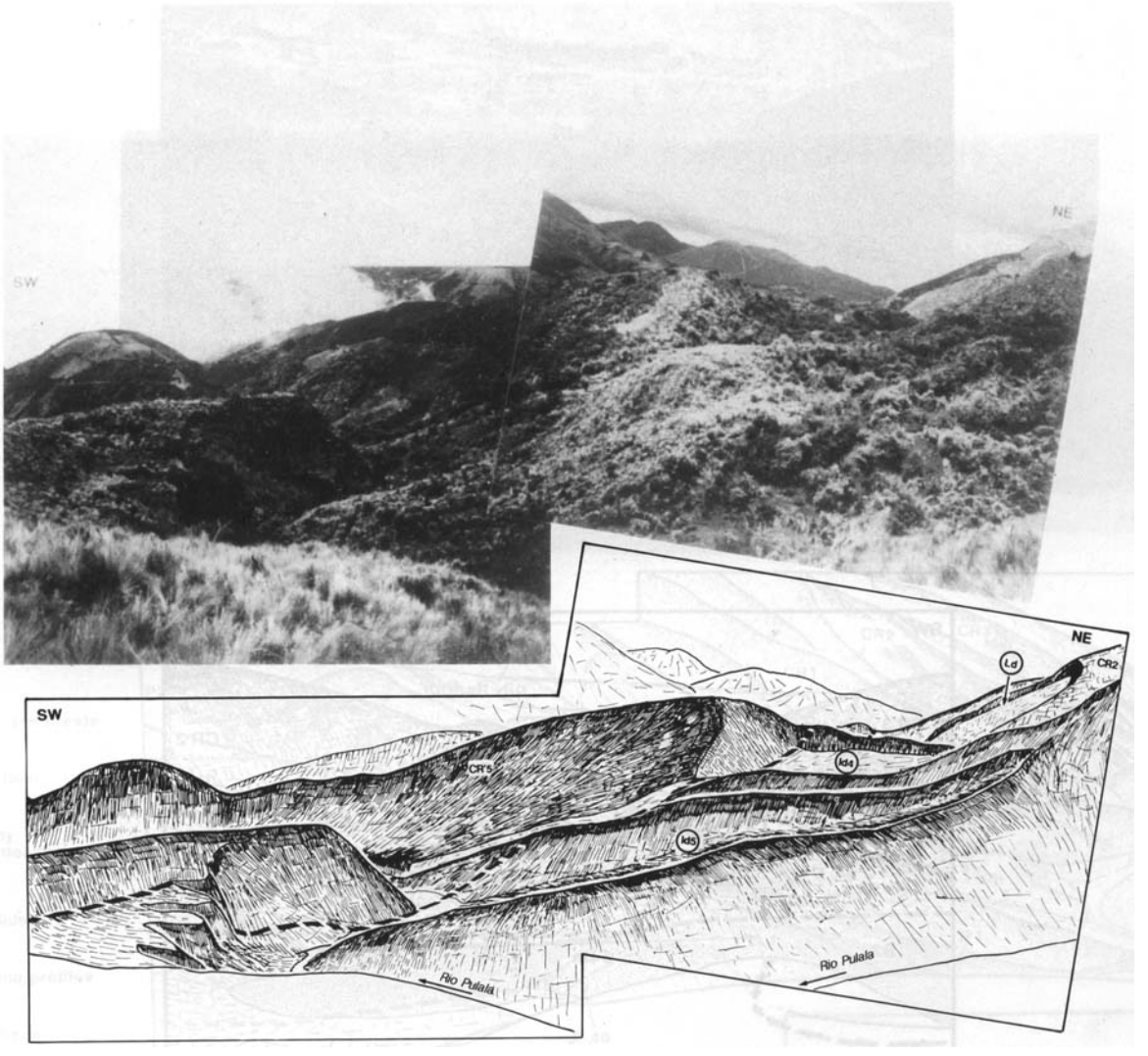

Figure 6. (a) West-looking view at the Quebrada Pulala where it is right-laterally offset by the fault. (b) Sketch of photograph 6(a).

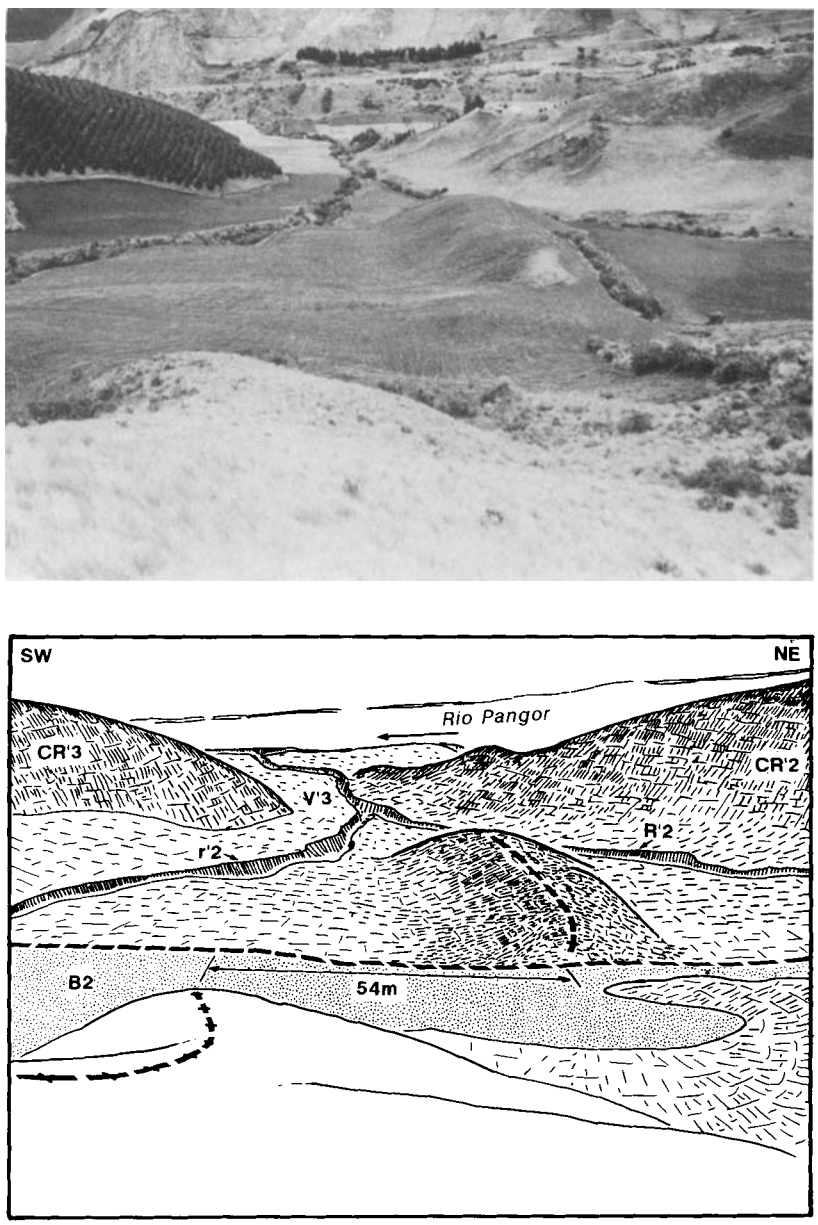

Figure 7. West-looking view of a small ridge offset by the fault (for location see valley V_3' in Fig. 3b).

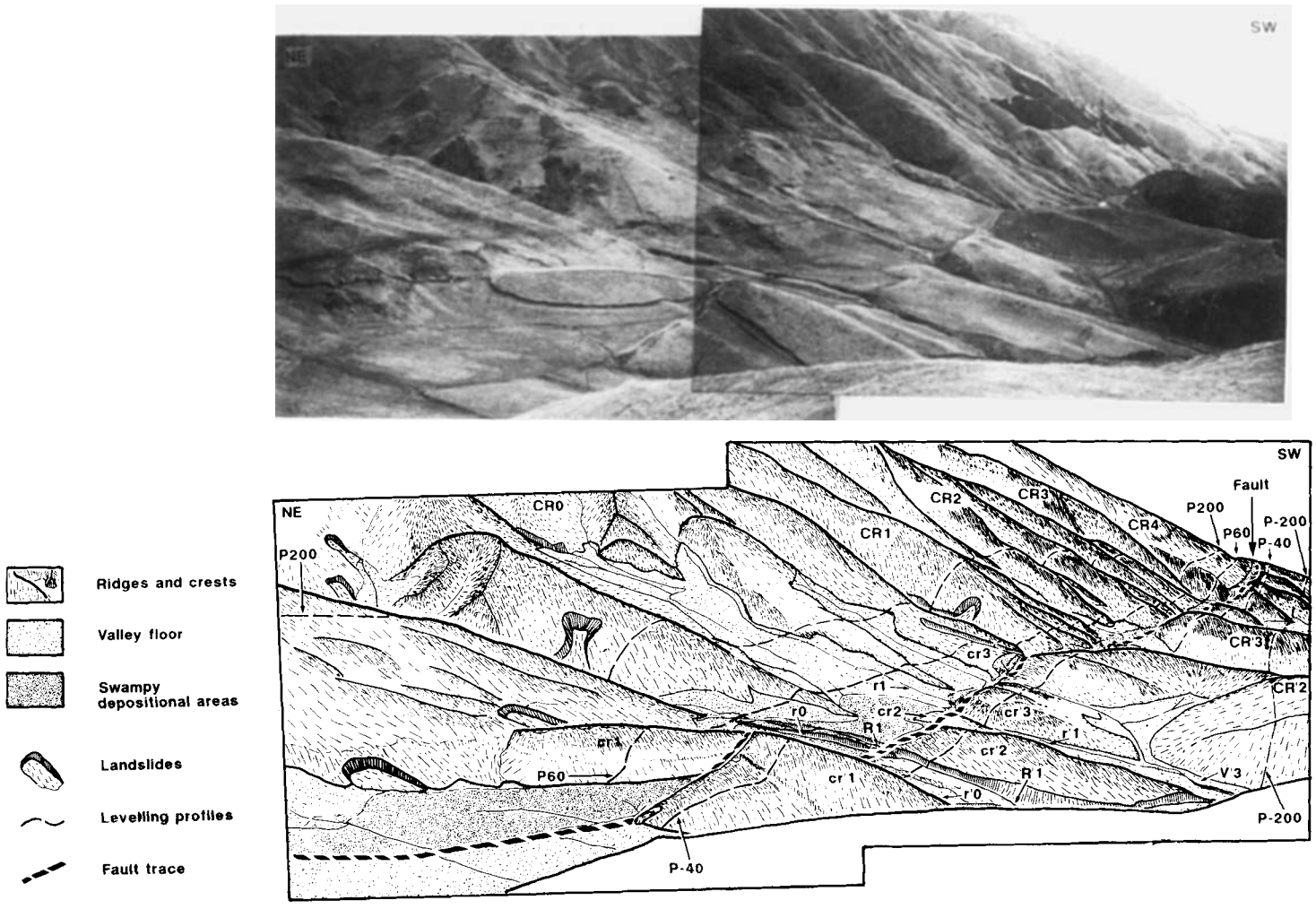

Figure 10. Offset crests along the northern fault zone. See Fig. 3(b) for location.

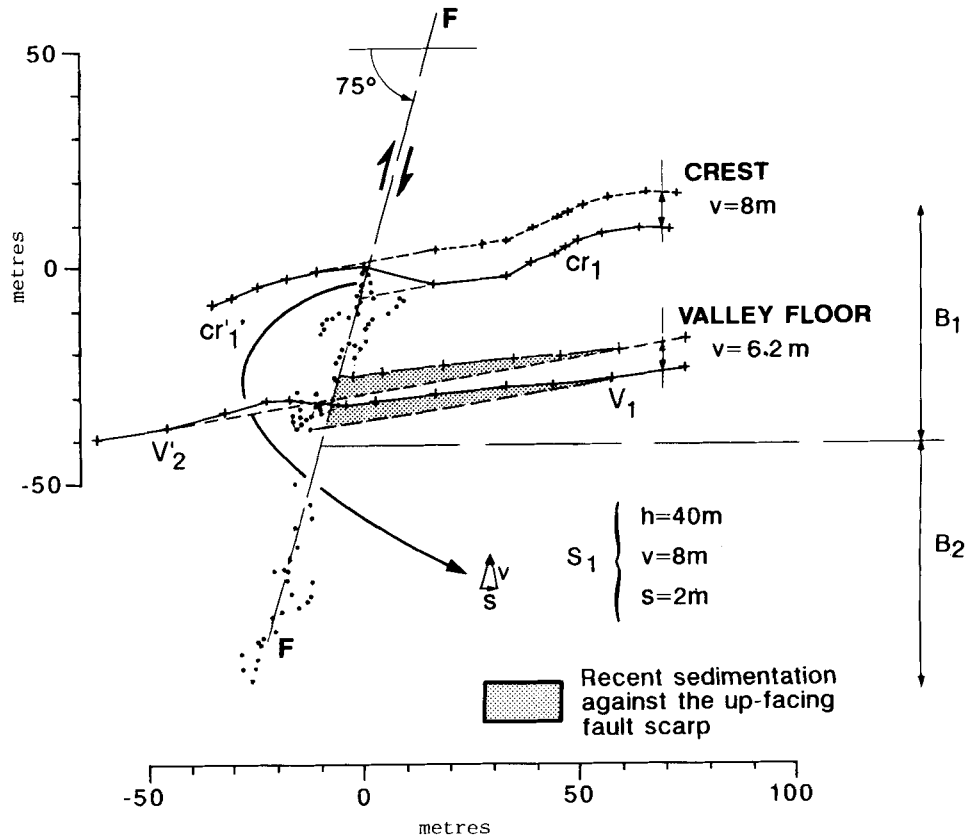

Figure 9. Projection in a vertical plane striking perpendicular to the fault strike. Dots are points of profiles P_u and P_d which bound the fault trace. It indicates a fault dip of 75° to the southwest. Crosses show the profiles levelled along the top of crest cr_1–cr'_1 and along the valley floor V_1. Restoration of a continuous crest across the fault requires an 8 m vertical component of slip. Such a displacement also restores a continuous valley floor if shaded area is interpreted as sediments dammed by the fault scarp.

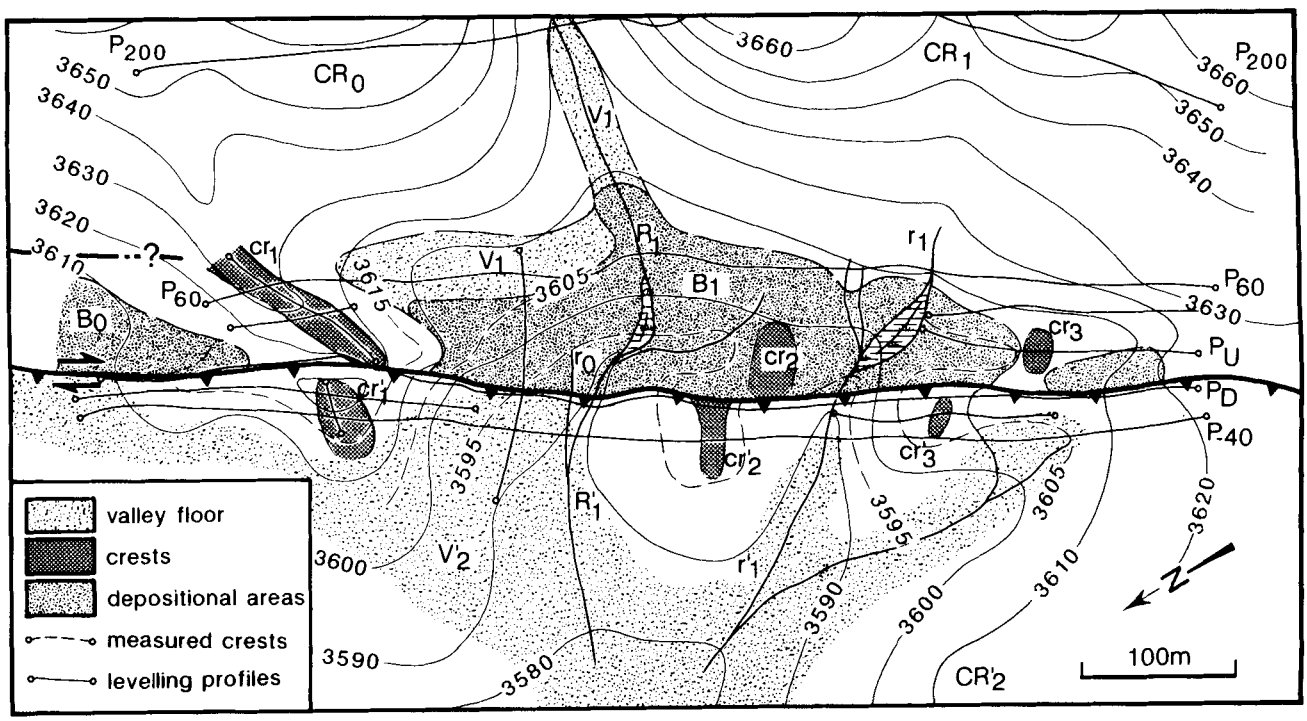

Figure 11. Detailed topographic and morphologic map of the northern part of the fault zone. See Fig. 3(b) for location. It was completed from the 1/50 000 topographic map combined with our levelling data and field observations.

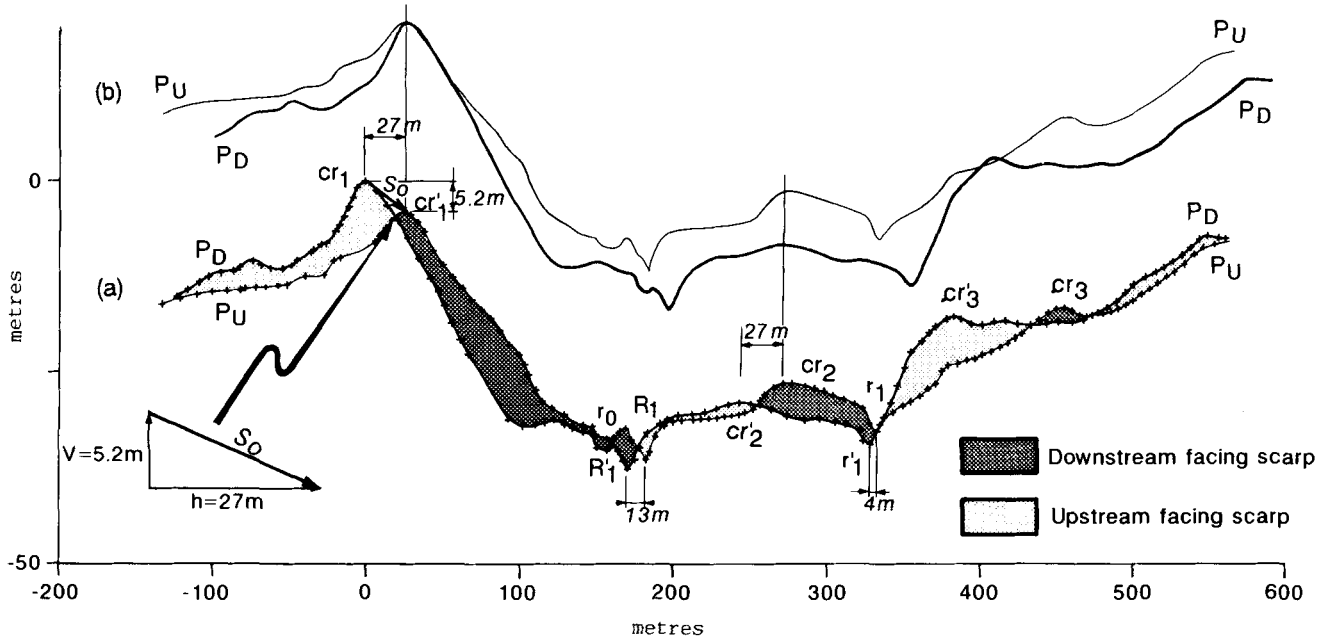

Figure 12. (a) Vertical projection in a plane parallel to fault strike of profiles P_u and P_d. A slip vector S_0 is deduced from the offset of crest cr_1–cr'_1. (b) Restored configuration according to slip vector S_0.

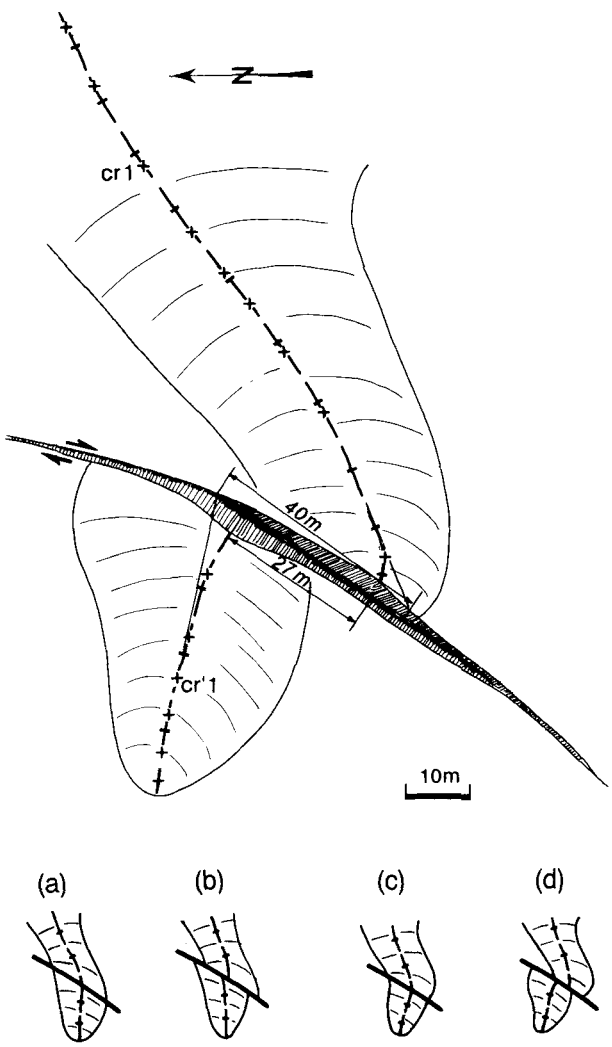

western block, were run 60 metres and 40 metres, respectively, away from the fault trace, because flat depositional areas sometimes extending more than 60 metres away from the fault. The topography would have shown less contrast on a profile run closer to the fault. The two profiles were projected on a vertical plane parallel to the fault strike (Fig. 15). At this distance from the fault trace, azimuthal corrections may be significant. The average strike of each crest or river has been determined from the whole set of profiles run parallel to the fault trace or on the aerial view. Obliquities were corrected for by extrapolating the structures onto the fault trace as shown in Fig. 15 (inset). Many crests of about the same size as cr_1–cr'_1, such as the one shown in Fig. 7, and many entrenched streams are offset between 32 m and 54 m, with a mean value of 41.5 m (Fig. 15) and a standard deviation, σ, of 6 m. The clustering of these measurements suggests that the morphological markers considered have formed synchronously during a relatively brief morphogenetic event.

Although the number of measurements is small, this 11-point series suggests that, assuming normally distributed errors (which seems a reasonable approximation), the 95 per cent confidence interval on an individual measurement has a width of 24 m (4σ). We expect this uncertainty to scale with

Figure 13. Mapview of crest cr_1–cr'_1. Crosses are points levelled along the top of the crest. It shows a net offset of about 27 m at the fault trace. The sigmoidal shape of the crest suggests that it has recorded a larger cumulative offset. Extrapolating the crest onto the fault trace yields about 40 m. We propose the following scenario which involves two major morphogenetic episodes: (a) the crest had been shaped as a relatively straight and continuous feature across the fault; (b) it was later offset by faulting, reshaped as a continuous, sigmoid crest at time of intense erosion (c) and again offset by faulting (d).

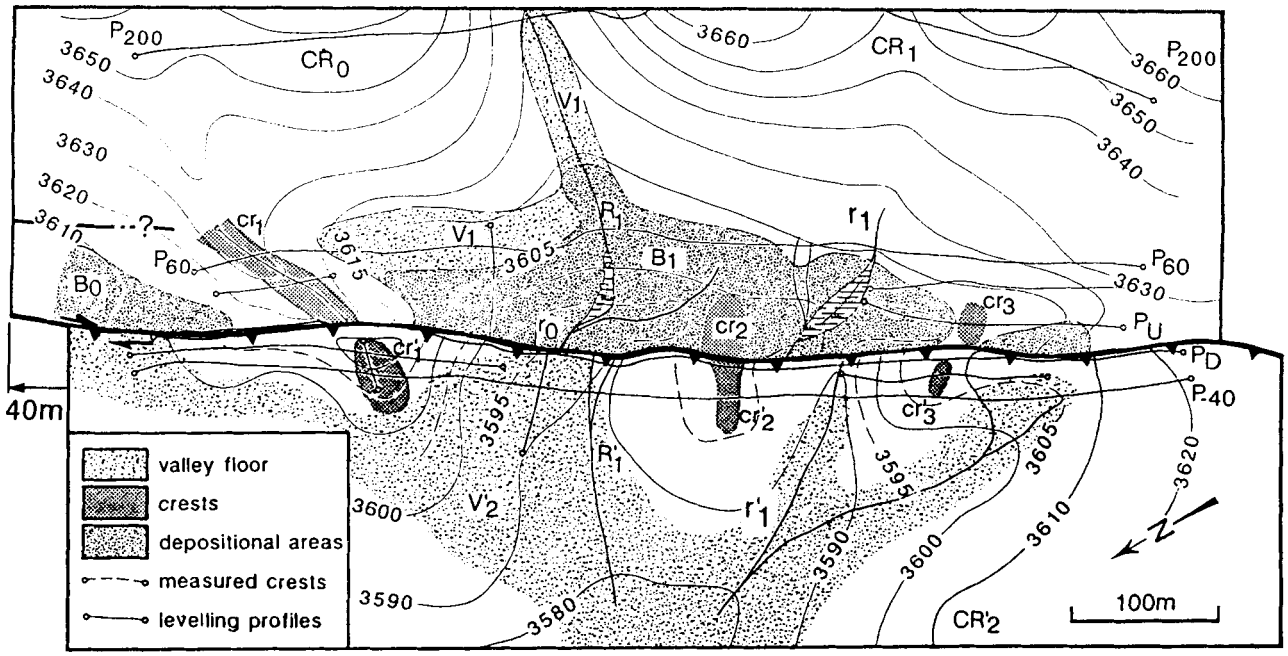

Figure 14. Restored configuration of the map of Fig. 12 for a 40 m strike–slip fault displacement.

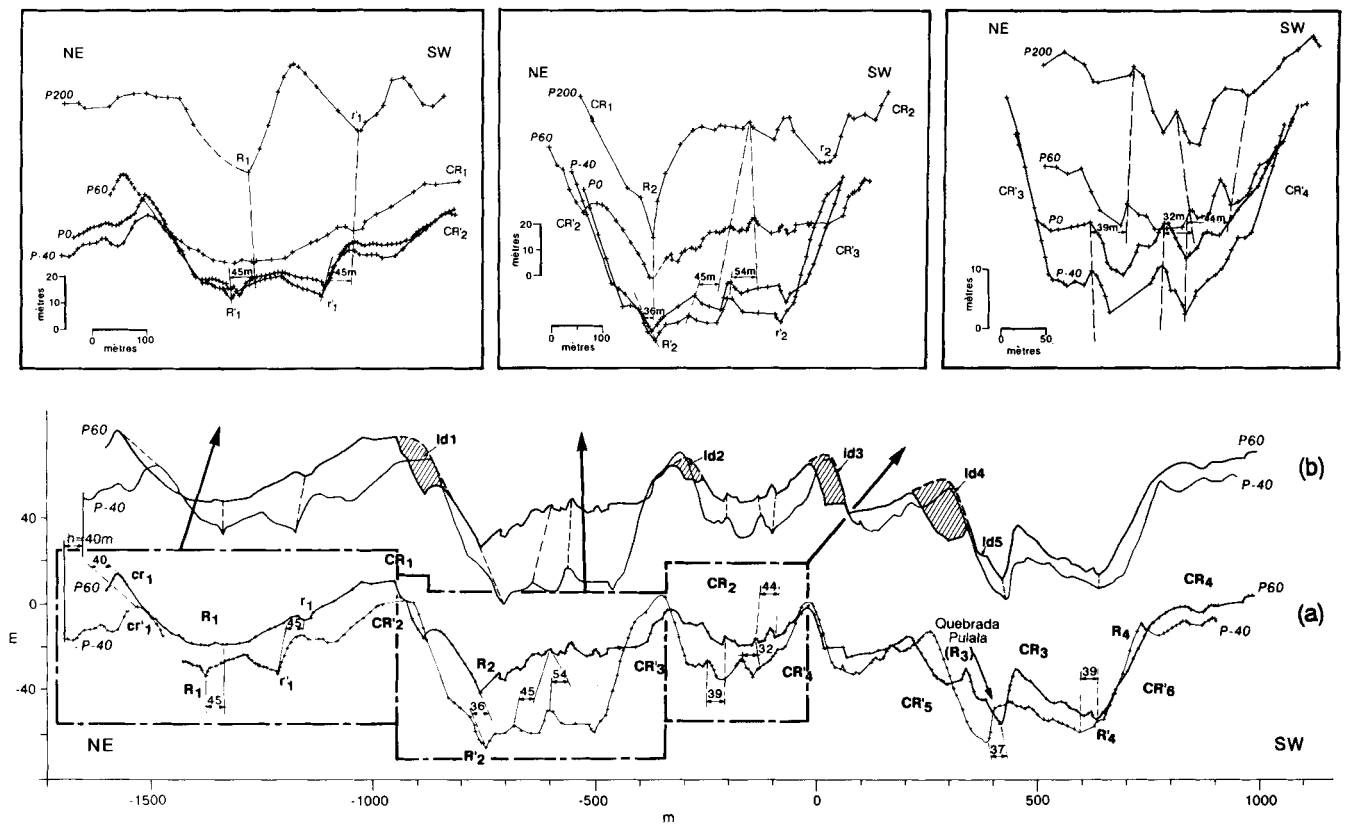

Figure 15. (a) Vertical projection in a plane striking parallel to fault trace of profiles P_{60} and P_{-40} (see Fig. 8 for location). Most minor ridges show offsets between 32 m and 54 m. Because these features are not strictly perpendicular to the fault strike, azimuthal corrections are accounted for graphically as shown in inset figures. It yields a mean value of 41.5 ± 4m. (b) Restored configuration of profiles P_{60} and P_{-40} for a 41.5 m fault offset. See discussion in text.

the characteristic dimension of the morphological feature rather than with the amount of displacement. Here the characteristic spacing of the valley and ridges is of the order of 150 m. The 95 per cent confidence interval on the measurement of an offset would thus have a width of about 20 per cent of the characteristic dimension of the morphological marker. The 95 per cent confidence interval on the 41.5 m mean offset, derived from 11 independent measurements, would be 41.5 ± 4 m, i.e. with a width of $4\sigma/\sqrt{11}$. We must, however, be aware that there might be some unaccounted source of errors due to the morphological evolution of the offset features, to the choice of these markers, or to variation of the cumulative slip along the fault strike. In the following, because the number of measurements is generally too small for well-constrained statistics, the confidence interval on a mean offset is estimated by assigning each individual measurement an uncertainty equal to 20 per cent of the characteristic width of the morphological marker considered. If the obtained uncertainty appears to be smaller than $2\sigma/\sqrt{n}$, where n is the number of measurements and σ the standard deviation of the measurements, then it will be corrected to this latter value.

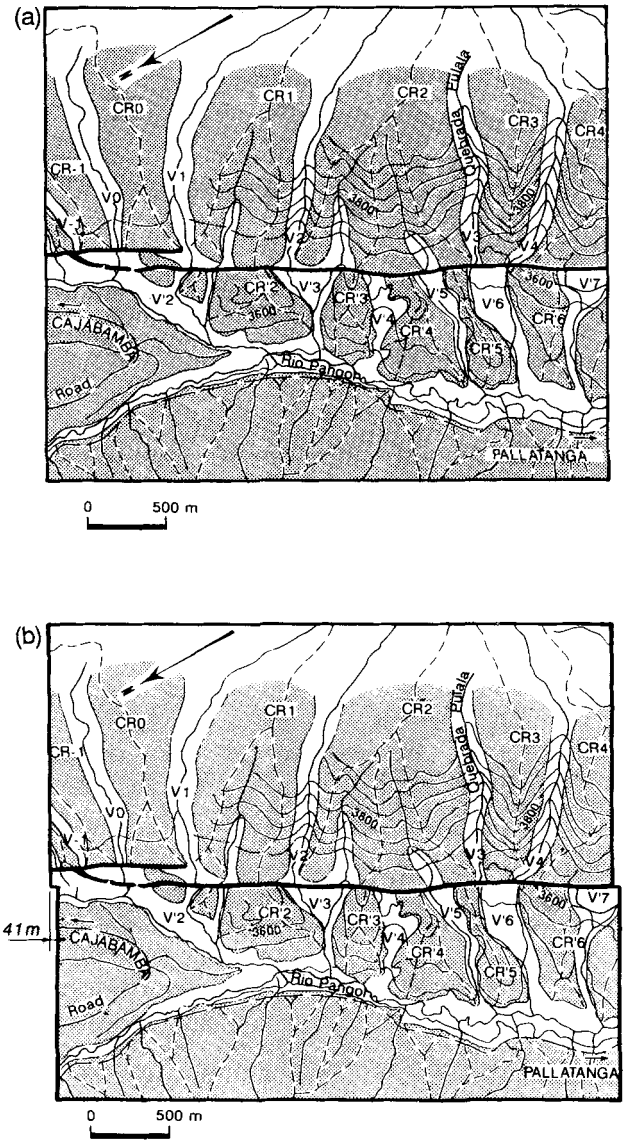

Figure 16. Restored configuration of map of Fig. 3(b) for a 41.5 m fault offset. Note that, at this scale, the landslides which affect the major crests close to the faults are not seen.

At first glance, there is no clear evidence that the major crests, notated CR_i, have recorded the 40 m offset. In Fig. 15, they rather appear to be continuous across the fault. Actually, this continuity is only apparent because most of these crests have been reshaped by large landslides. For example, we noticed that major landslides had occurred in front of the downstream valley of the Quebrada Pulala (ld_4 and ld_5 in Figs 3b, 6 and 15). The highest downhill-facing fault scarps which should have formed as a result of the right-lateral offset of the major crests seem to have experienced similar landslides (Fig. 3b). Once this phenomenon was pointed out, the location and size of these probable landslides, hence the approximate unaltered shape of the crests, could be inferred (dashed areas in Fig. 15) by comparing P_{-40} and P_{60} restored to the initial configuration corresponding to the 41.5 m fault displacement. Downhill-facing high and steep scarps submitted to underground water seepage are indeed particularly vulnerable to mass movement. By contrast uphill-facing scarps have been better preserved or buried by sedimentation. In order to check this inference, the topographic and morphologic map of Fig. 3(b) has been cut along the fault trace and restored to the configuration corresponding to a 41.5 m offset (Figs 16 a and b). The major crests and valleys actually appear to be continuous in his configuration. Thus, paradoxically, small structures still show relatively clear offset whereas major crests have been reshaped to apparent continuous features by catastrophic erosional processes. This example illustrates how local erosional processes can account for poor restorations of morphological offsets.

Long-term offsets

We ran topographic profiles 200 metres away from the fault trace on both sides (P_{200} and P_{-200} in Fig. 8) in order to estimate the long-term offsets responsible for the large-scale morphologic discontinuities. A particular point was to investigate which valley in the upstream fault block, most probably fed the now-abandoned valley V_4' in the downstream fault block. Because only parts of these profiles were levelled in the field, they were completed from the 1/50 000 topographic map. A projection on a vertical plane parallel to the fault strike is shown in Fig. 17. Two configurations are found to put V_4' in continuity with a similarly large valley in the upstream fault-block.

In the first configuration, V_4' is paired with V_3, 525 m away (Fig. 17a). Other correlations between similarly large crests and valleys on both sides of the fault could be consistent with about the same fault displacement. For example V_5' is paired with V_4, 580 m away. The corresponding offsets range between 525 m and 680 m (Fig. 17a), with a mean value of 590 m and a standard deviation of 65 m derived from four independent measurements. According to the method proposed above and given that the characteristic dimension of the markers is around 500 m, we get a 95 per cent confidence interval of 590 ± 65 m. Fig. 18(a) shows the reconstructed configuration of the map of Fig. 3(b) for a

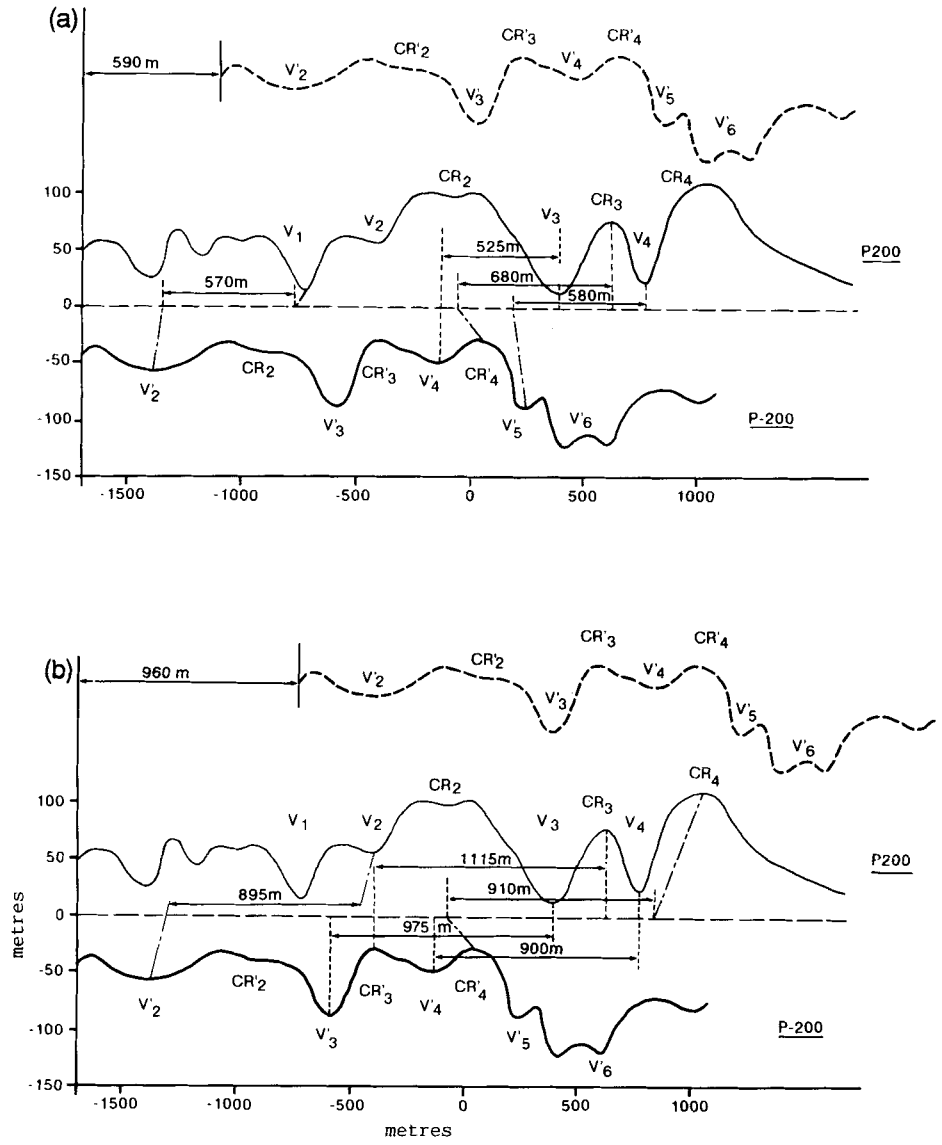

Figure 17. Vertical projection in a plane striking parallel to fault trace of profiles P_{200} and P_{-200} (see Fig. 8 for location). Two different restored configurations appear to put the large wavelength topographic features on both sides of the fault into correspondence. In particular the now-abandoned valley V_4' in the downstream fault block can correlate with either valley V_3 (a) or V_4 (b) in the upstream fault block. Similar correspondence between valleys and crests on each side of the fault can be found to be consistent with the two possibilities. The measured offsets cluster either around 590 ± 65 m or 960 ± 70 m. The corresponding restored positions of profile P_{-200} (dashed lines), with respect to profile P_{200} are shown in (a) and (b), respectively.

590 m offset. It appears that only one large valley, V_6', is not paired. V_6' might have not existed at the time corresponding to this configuration; it could have formed more recently when the configuration was that of Fig. 16(b) on which V_6' is facing valleys V_3 and V_4 in the upstream fault block. Another possibility is that V_6' already existed at the time of the configuration of 17(a) and was already an offset and abandoned valley. This would indicate a cumulative offset, recorded in the morphology, larger than 590 m.

In the second configuration, V_4' is paired with V_4, 900 m away (Figs 17b and 18b). Other correlations between large crests and valleys on both sides of the faults would also be consistent with about the same fault displacements. Offsets ranging between 895 m and 1115 m are obtained (Fig. 17b), with a mean value of 960 m and a standard deviation of 80 m derived from five measurements. The 95 per cent confidence interval on this measurement would be 960 ± 70 m. As seen in Figs 17(a) and 18(b) the 960 m offset also provides a satisfactory configuration in which V_5' is not however, paired. This valley could have formed later when it was facing V_3 or V_4 on the upstream side of the fault.

There is thus no definite evidence that the major crests and valleys have recorded 590 or 960 m since they were carved across the fault. The two solutions could thus correspond to the configurations at times of two different major but brief morphogenetic episodes.

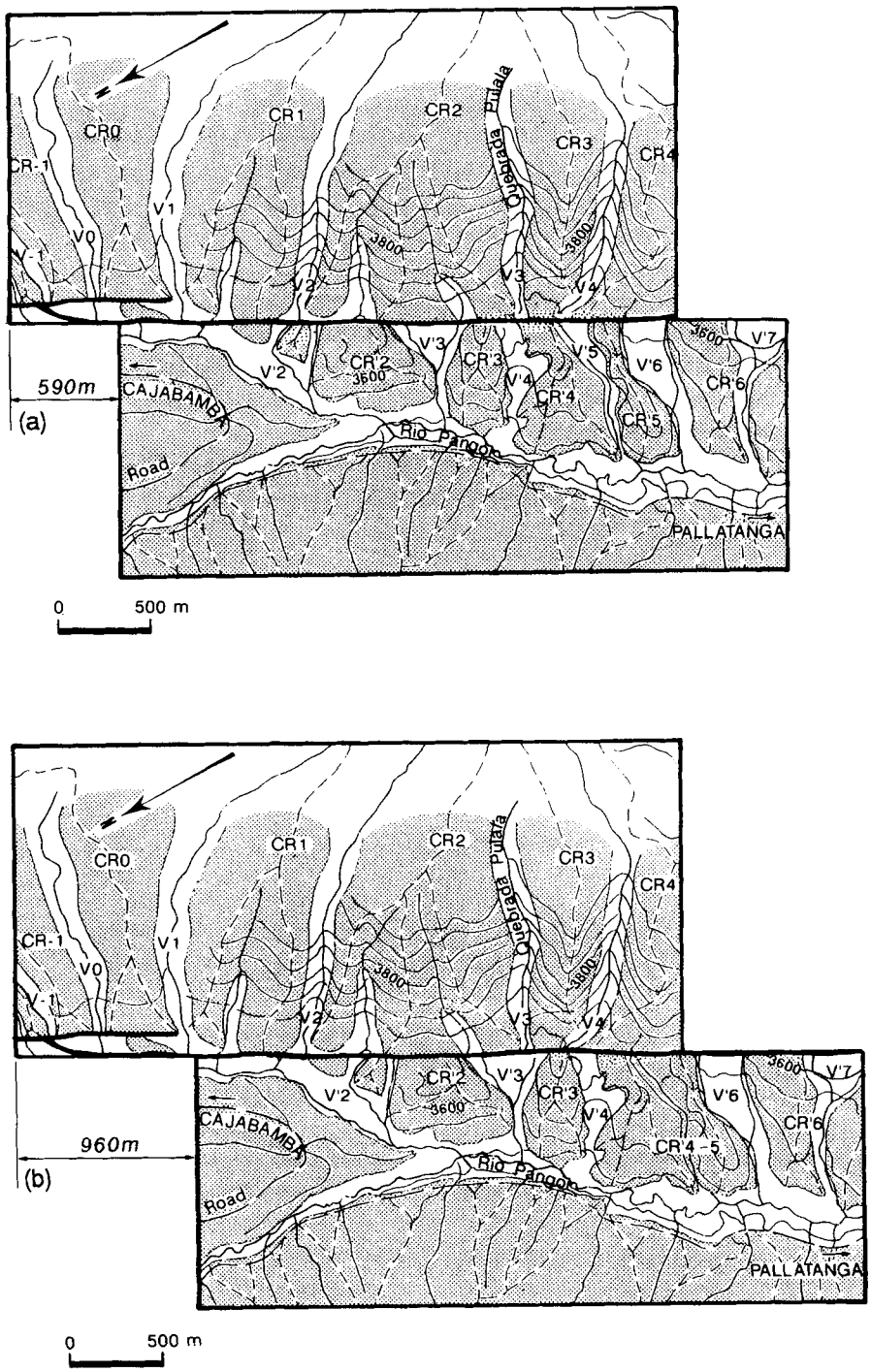

Figure 18. Restored configurations of map of Fig. 3(b) for 590 m (a) and 960 m (b) fault offset. See discussion in text.

CORRELATION WITH CLIMATIC EVENTS

The average slip rate on the Pallatanga fault may be deduced from measured offsets only if ages can be assigned to the offset morphologic features. Dating of the morphology is notably difficult. As for the study of the Chang Ma fault by Peltzer *et al.* (1988), it appears that the morphology has recorded offsets that cluster around a few distinct values, depending on the size of the morphologic features considered. The fault scarp, which marks the fault trace in the topography, is related to a 27 ± 11 m right-lateral offset. Small crests and valleys, with a typical width of a few tens of metres, appear to have been offset by about 41.5 ± 4 m, but have been partly reshaped by erosion processes when the configuration was that corresponding to the 27 m of offset. Abandoned valleys truncated against the fault indicate that the morphology has recorded even larger fault offsets. Valleys and ridges with a typical width of a few

hundred metres have indeed been found to correlate across the fault, suggesting a fault displacement of 590 ± 65 m or 960 ± 70 m. Our interpretation is that slip on the fault, which appears as a continuous process over the long intervals (several thousands years), has been punctuated by climatic events, each of which would have formed continuous and coeval topographic features across the fault. The slip rate on the fault may thus be deduced from the correlation of the displacements recorded in the morphology with the major climatic events which could have left marks in the morphology.

The studied fault segment lies at the base of a range that reaches elevations above 4100 m on bear traces of extinct glaciers (Fig. 2). The present-day snow line on the Chimborazo, Carihuairazo and Altar volcanoes, which all lie within about 40 km of the Pallatanga fault segment, follows the 4900 m elevation contour line, and active glacial tongues extend down to elevations between 4600 m and 4850 m (Clapperton 1987). The snow-line during the Würm glaciation was generally about 1000 m lower than at present for latitude between 30°S and 30°N (Broecker & Denton 1990) and has been estimated at about 4200 m between 12 and 10 kyr BP in Central Ecuador (Clapperton 1987). It is thus likely that the major change in the nature and rates of recent surface-shaping processes in this area have been controlled by glacial pulses, and that during the Würm period, the site lay well within the periglacial domain so that intense surface erosion would have smoothed out any small-scale morphological discontinuity across the fault zone.

The timing and extent of the Quaternary glaciations in Ecuador (Van Der Hammen 1981; Clapperton 1987) appear to be similar to those in Peru (Clapperton 1972; Lliboutry *et al.* 1977; Fornari, Herail & Laubacher 1982) and Colombia (Gonzalez, Van Der Hammen & Flint 1965; Thouret *et al.* 1993). In particular, the most conspicuous group of abandoned moraines, which reach down to elevations about 3650 m on the Chimborazo, Carihuairazo and Altar volcanoes, are thought to be terminal Würm moraines. They would correspond to late-glacial advances that have been observed regionally and dated at between 12 and 10 kyr BP by Clapperton (1987), between 13.3 kyr and 10 kyr BP by Thouret (1989), between 10 and 9.5 kyr BP by Van der Hammen (1981), and between 10.9 and 10 kyr BP by (Mercer & Palacios 1977; Wright 1984). We infer the 41.5 ± 4 m offset to post-date this latest Würm glacial advance which, according to the available dates, can be assigned a maximum age of about 11 kyr BP. The calibration proposed by Bard *et al.* (1991) for ^{14}C ages, yields a calendar age of about 13 kyr BP. This age implies a Holocene minimum slip rate on the Pallatanga fault of 2.9 mm yr^{-1}.

Some minor glacial advances are known to have occurred in Ecuador, Colombia and Peru during the Holocene period (Clapperton 1972, 1983, 1987; Lliboutry *et al.* 1977; Thouret & Van der Hammen 1981; Thouret *et al.* 1993). However, none of them could have induced a sufficient lowering of the snow-line for glaciers to have formed at elevations below 4600 m (Clapperton 1987). We, therefore, consider that the 41.5 ± 4 m should be assigned an age older than that of these minor glacial advances. Given that the glacial cirques in the Pallatanga fault area are relatively small, with maximum length of a few kilometres, the glacial recession must have been rapid so that the periglacial environment in this area probably disappeared rather rapidly in the early Holocene. On the basis of the age of the latest moraine and on the timing of the global warming in the early Holocene (e.g. Fairbanks 1989), we propose a minimum calendar age of about 10 kyr for the 41.5 ± 4 m offset, yielding a maximum Holocene slip rate of 4.6 mm yr^{-1}. The Holocene slip rate on the Pallatanga Fault is thus estimated to be in the range 2.9–4.6 mm yr^{-1}.

A Middle Holocene minor glacial pulse has been identified in Ecuador (Clapperton 1987), Colombia (Thouret & Van der Hammen 1981; Thouret *et al.* 1993) and Peru (Clapperton 1972; Lliboutry *et al.* 1977). It has been dated at about 7000 BP by Lliboutry *et al.* (1977), between 6000 and 4000 BP by Clapperton (1972) and between 7400 and 6000 BP (Thouret & Van der Hammen 1981). Although this event must have had minor morphogenetic effects compared to the early Holocene deglaciation, it might have induced renewed periglacial erosion in the studied fault zone. We thus suspect that this event could correlate with the 27 ± 11 m morphological offset. Assigning a minimum age of 4000 yr BP and a maximum age of 6000 yr BP (which becomes 7000 yr BP if we apply the calibration proposed by Bard *et al.* 1991), implies a slip-rate between 2.6 mm yr^{-1} and 5.9 mm yr^{-1}, consistent with the proposed Holocene slip rate of 2.9–4.6 mm yr^{-1}.

The long-term fault displacements of 590 ± 65 m and 960 ± 70 m were measured from the offsets of long-wavelength morphologic features which could have been inherited from major glacial pulses older than the last glacial maximum. A possible such event is the glacial termination that occurred at the beginning of the last interglacial period which has been identified in marine sediment records (Imbrie *et al.* 1984; Martinson *et al.* 1987; Broecker & Denton 1990) and which can be assigned an age of about 120–135 kyr (Lambeck & Nakada 1992). Van Der Hammen (1981) proposes a youngest possible age of 130 kyr BP in Ecuador. There is no definitive argument suggesting that the long-term offset of 590 ± 65 m should correspond with this event. However, the fact that it implies a strike–slip rate of about 4–5 mm yr^{-1} in rough agreement with the 2.9–4.6 mm yr^{-1} Holocene slip rate, makes it an attractive hypothesis. Furthermore, taking the 2.9–4.6 mm yr^{-1} rate to be representative of the mean slip rate in the long term, the 960 ± 70 m offset would then correspond to the previous major glacial termination (Fig. 19), which has also been identified in marine records and dated at about 240–250 kyr BP (e.g Imbrie *et al.* 1984; Martinson *et al.* 1987).

The plot in Fig. 19 illustrates how the measured morphological offsets and the hypothesized ages allow a uniform slip rate. This correlation supports the inference that the two or three latest glacial terminations can be associated with major morphogenetic episodes that have reshaped a continuous morphology across the fault zone.

We exclude the possibility that the correlation between offsets and glacial terminations could be an artefact due to the regular spacing of the valleys and to the periodic occurrence of glacial pulses. If the spacing between two adjacent valleys of similar size is DX, the restored morphology for strike–slip displacements of DX, $2DX$ would

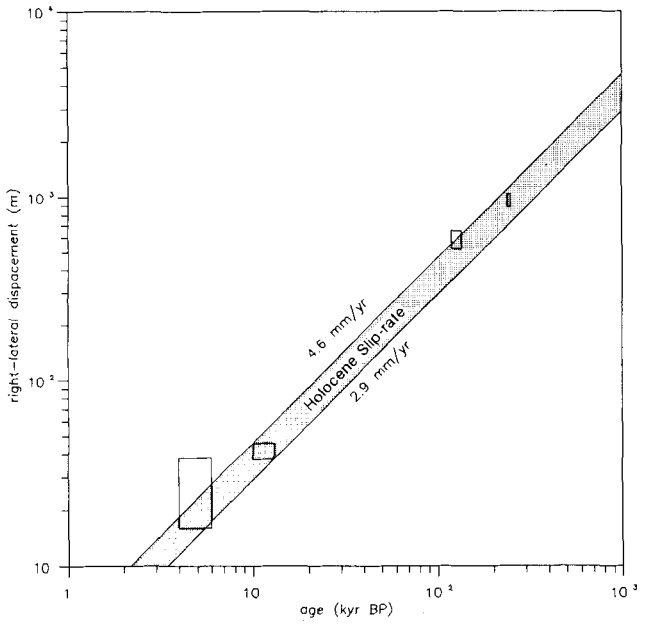

Figure 19. Measured lateral offsets of the morphology along the Pallatanga Fault plotted against estimated ages. The 27 ± 11 m, 41.5 ± 4 m, 590 ± 65 m and 960 ± 70 m cumulative offsets have been assigned ages of 4–7, 10–13, 120–135 and 240–250 kyr BP respectively.

appear roughly continuous (Gaudemer *et al.* 1989). Let $\mathrm{D}T$ be the return period of glacial terminations, the two periodic signals would then fall into correspondence for an apparent slip rate of $\mathrm{D}X/\mathrm{D}T$. In the present study, we have given evidence that a long-term fault offset of at least 590 m must have occurred on the fault to account for major morphological discontinuities across the fault zone. The correlation between the 960 ± 70 m offset and the glacial termination at 240 kyr might be fortuitous, but the fact that it corresponds to a slip rate in agreement with the independently determined slip rate for the Holocene period strongly supports our inference of an actual correlation.

SEISMIC BEHAVIOUR

In the field, we didn't observe any fresh breaks what would suggest a seismic event. Yet, the morphology of the fault scarps attests to sustained fault slip. Given that the fault segment extends over a distance of more than 25 km (Fig. 2), it has the potential for generating a large damaging earthquake with $M_S > 7$. It is probable that in such a humid and vegetated area, a seismic break would be rapidly smoothed out, so that we do not exclude that this fault could have been the site of a recent earthquake. No historical or instrumental earthquake is known to have occurred on that particular fault. The only large event reported in this area is the 1797 February 4 (11 MKS) Riobamba earthquake (CERESIS 1985; Winter 1990) which devastated the city of Riobamba and numerous nearby cities in the Interandean Depression (Fig. 20). At Cajabamba, it triggered a huge landslide which dammed the valley. The proposition that this earthquake could have activated the Pallatanga fault (Winter 1990) is a possibility although we cannot exclude that it could have been related to a thrust event in the Interandean Depression.

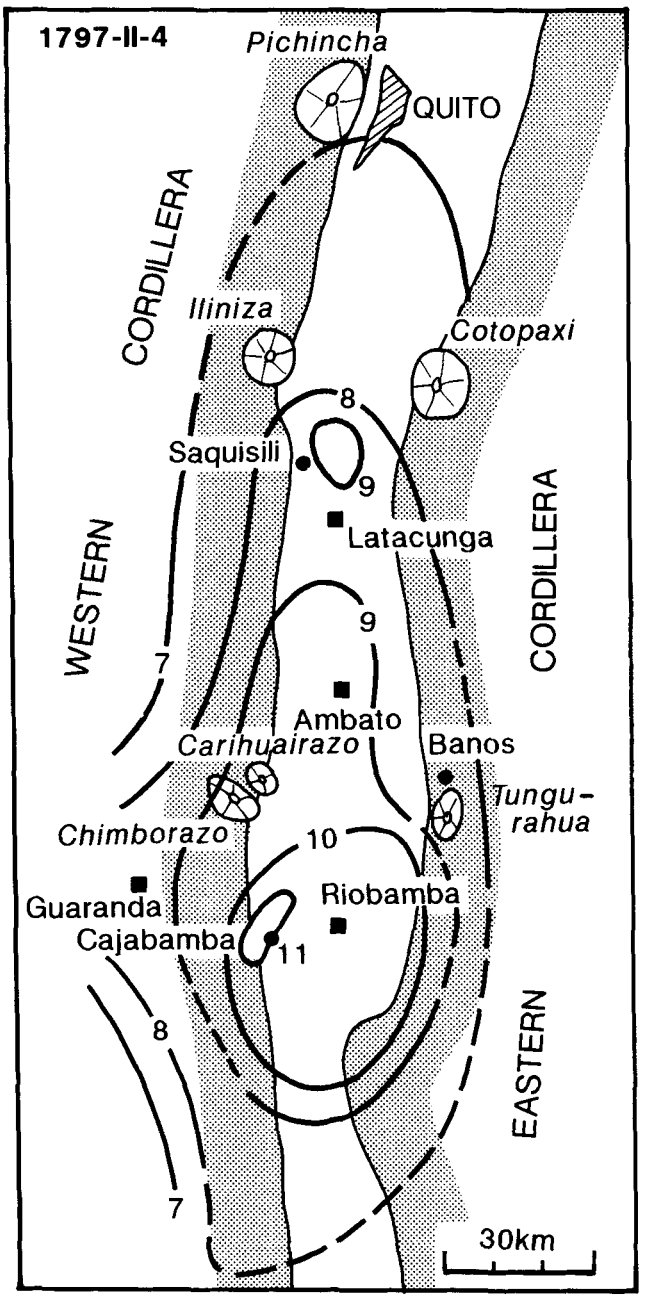

Figure 20. Distribution of damages caused by the 1797 February 4 Riobamba earthquake (from Winter 1990).

CONCLUSION

The fault plane is shown to strike N30°E and dip 75° to the northwest. Numerous measurable offsets of morphological features indicate unambiguous right-lateral strike-slip on the fault. The slip vector projected on the fault plane shows a slight reverse component with a pitch of about 11.5°SW. Offset morphological features which can be inferred to be of early Holocene age indicate a mean Holocene slip rate of 2.9–4.6 mm yr^{-1}. This rate is further corroborated by a 27 m short-term offset, which would correlate with a middle Holocene morphoclimatic event, and by long-term offsets of 590 m and 960 m, which would correlate with the three last

glacial terminations. These correlations show that the morphology does not evolve continuously at the scale of a few tens to a few hundred thousand years but appears to result from the superpositon of distinct morphogenetic events that seem to correspond to the major glacial terminations. This observation was possible because, owing to the fault activity, the morphologic traces of these events are not superposed as it would be the case in a stable tectonic context.

ACKNOWLEDGMENTS

We thank Peter Molnar and Bob Yeats for constructive and thorough reviews. This study has benefited from fruitful discussions with Gilles Peltzer, Yves Gaudemer, Bertrand Meyer, Rolando Armijo and Paul Tapponnier. Special thanks are due to Guy Aveline for the illustration. This study was supported by IFEA and ORSTOM (Contract IPGH-EPN-CLIRSEN-ORSTOM-IFEA in Ecuador).

REFERENCES

Armijo, R., Tapponnier, P., Mercier, J. L. & Han, T. L., 1986. Quaternary extension in southern Tibet: field observation and tectonic implications, *J. geophys. Res.*, **91,** 13803–13872.

Barazangi, M. & Isacks, B. L., 1976. Spatial distribution of earthquakes and subduction of the Nazca plate beneath South America, *Geology,* **4,** 686–692.

Bard, E., Hamelin, B., Fairbanks, R. G. & Zindler, A., 1991. Calibration of the ^{14}C timescale over the past 30,000 years using mass spectrometric U–Th ages from Barbados corals, *Nature,* **345,** 405–409.

Benitez, S., 1986. Sintesis geologica del Graben Jambeli, *IV Cong. Ecuat. de Geol., Min. y Petrol., Octubre 1986, Quito,* T1, 137–160.

Bourgeois, J., Toussaint, J. F., Gonzales, H., Orrego, A., Azema, J., Calle, B., Desmet, A., Murcia, A., Pablo, A., Para, E. & Tournon, J., 1985. Les ophiolites des Andes de Colombie: évolution structurale et signification géodynamique, in *Géodynamique des Caraïbes,* pp. 475–493, ed., Mascle, A., Technip., Paris.

Broecker, W. & Denton, G., 1990. Les cycles glaciares, *Science,* **149,** 62–71.

Campbell, C. J., 1974a. Ecuadorian Andes, in *Mesozoic–Cenozoic orogenic belts, data for orogenic studies,* pp. 725–732, ed. Spencer, A. M., Geol. Soc., London.

Campbell, C. J., 1974b. Colombian Andes, in *Mesozoic–Cenozoic Orogenic Belts, Data for Orogenic Studies,* pp. 705–724, ed. Spencer, A. M., Geol. Soc., London.

Case, J. E., Barnes, J., Paris, G., Gonzalez, M. & Vina, A., 1973. Trans Andean geophysical profile, southern Colombia, *Geol. Soc. Am. Bull.*, **84,** 2895–2904.

Case, J. E., Duran, L. G., Lopez, A. & Moore, W. R., 1971. Tectonic investigations in western Colombia and eastern Panama, *Geol. Soc. Am. Bull.*, **82,** 2685–2712.

Chinn, D. S. & Isacks, B. L., 1983. Accurate source and focal mechanisms of shallow earthquakes in western South America and in the New Hebrides island arc, *Tectonics,* **2,** 259–563.

CERESIS, 1985. Centro regional de sismologia para America del Sur, *Catalogo de terremotos para America del Sur,* Vol. 6.

Clapperton, C. M., 1972. The pleistocene moraine stages of west-central Peru, *J. Glaciol.*, **11, 62,** 255–263.

Clapperton, C. M., 1983. The glaciation of the Andes, *Quat. Sci. Rev.*, **2,** 83–155.

Clapperton, C. M., 1987. Glacial geomorphology, Quaternary glacial sequence and paleoclimatic inferences in the Ecuadorian Andes, in *International Geomorphology 1986 Part II,* pp. 843–870, ed. Gardiner, V., John Wiley & Sons Ltd, New York.

Clark, M. N., 1970. Some characteristics of the most recently active traces of the Garlock fault, *Geol. Soc. Am. Abstr. Programs,* **2, 82,** 1970.

Fairbanks, R. G., 1989. A 17000-yr glacio-eustatic sea level record: influence of glacial melting rates on the Younger Dryas event and deep-ocean circulation, *Nature,* **342,** 637–642.

Faucher, B. & Savoyat, E., 1973. Esquisse géologique des Andes d'Equateur, *Rev. Géogr. Phys. Géol. Dyn.*, **2, XV,** 1–2: 115–142.

Feininger, T. & Bristow, C. R., 1980. Cretaceous and Paleogene geologic history of coastal Ecuador, *Geol. Rdsch.*, **69, 3,** 849–874.

Feininger, T. & Seguin, M. K., 1983. Simple Bouguer gravity anomaly field and the inferred crustal structure of continental Ecuador, *Geology,* **11,** 40–44.

Fornari, M., Herail, G. & Laubacher, G., 1982. El oro en la Cordillera suroriental del Peru: el Placer fluvioglacial de San Antonio y sus relaciones con la mineralizacion primaria de la Rinconada, V Cong., *Latino–Americano Geologicano, Argentina,* **4,** 369–386.

Gaudemer, Y., Tapponnier, P. & Turcotte, D. L. 1990. River offsets and active strike–slip faults, *Ann. Tecton.*, **3,** 55–76.

Gonzales, E., Van Der Hammen, Th. & Flint, R. F., 1965. Late quaternary glacial and vegetational sequence in Valle de Lagunillas, Sierra Nevada del Cocuy, Colombia, *Leidse Geologische Mededelingen,* **32,** 157–182.

Hasenrath, S., 1981. *The Glaciation of the Ecuadorian Andes.* A. A. Balkema, Rotterdam.

Imbrie, J., Hays, J. D., Martinson, D. G., McIntyre, A., Mix, A. C., Morley, J. J., Pisias, N. G., Prelland, W. L. & Schackelton, N. J., 1984. The orbital theory of the Pleistocene climate: support from a revised chronology of marine $d^{18}O$ record, in *Milankovitch and climate,* part I, pp. 269–305, eds Berger *et al.*, D. Reidel Publ. Co., Dordrecht.

Kelleher, J. A., 1972. Rupture zone of large South American earthquakes and some predictions, *J. geophys. Res.*, **77,** 2087–2103.

Lanbeck, K. & Nakada, M., 1992. Constraints on the age and duration of the last interglacial period and on sea-level variations, *Nature,* **357,** 125–128.

Lavenu, A., 1986. Etude néotectonique de l'Altiplano et de la Cordillère Orientale des Andes Boliviennes, *thèse Doctorat d'Etat,* Université Paris-Sud, Orsay.

Lebrat, M., Megard, F. & Dupuy, C., 1985a. Pre-orogenic volcanic assemblages and position of the suture between oceanic terranes and South American continent in Ecuador, *Zbl. Geol. Paleont. Teil I,* H 9–10, 1207–1214.

Lebrat, M., Megard, F. & Dupuy, C., 1985b. Pre-orogenic volcanic assemblages and structure in the western Cordillera of Ecuador between 1°40′S and 2°20′S, *Geol. Rdsch.*, **74,** 685–713.

Lliboutry, L., Morales Arnao., B., Pautre, A. & Schneider, B., 1977. Glaciological problems set by control of dangerous lakes in Cordillera Blanca, Peru. I. Historical failures of morainic dams their causes and prevention. II. Movement of a covered glacier embedded within a rock glacier. III. Study of moraines and mass balances at Safuna, *J. Glaciol.*, **18,** 79.

Malfait, B. T. & Dinkelman, M. G., 1972. Circum Caribbean tectonic and igneous activity and the evolution of the Caribbean plate, *Geol. Soc. Am. Bull.*, **83,** 251–272.

Martinson, D. G. *et al.*, 1987. Age dating and the orbital theory of the ice ages: development of a high resolution 0 to 300 000 yr chronostratigraphy, *Quat. Res.*, **27,** 1–29.

McCourt, W. J., Apsden, J. A. & Brook, M., 1984. New geological and geochronological data from Colombian Andes: continental growth by multiple accretion, *J. Geol. Soc. Lond.*, **141,** 831–841.

Megard, F., 1987. Cordilleran Andes and Marginal Andes: a review of andean geology North of Arica elbow (18°), *Circum-Pacific orogenic belts and evolution of the Pacific Ocean basin,* eds, Monger, J. W. H. & Francheteau, J., *Geodynamics Series,* **18,** Am. geophys. Un., Washington, DC.

Mercer, J. H. & Palacios, O., 1977. Radiocarbon dating of the last glaciation in Peru, *Geology,* **5,** 600–604.

Peltzer, G., Tapponnier, P., Gaudemer, Y., Meyer, B., Shunmin, G., Kelun, Y., Zhitai, C. & Huagung, D., 1988. Offsets of late quaternary morphology, rate of slip, and recurrence of large earthquakes on the Chang Ma Fault (Gansu, China), *J. geophys. Res.,* **93, 87,** 7793–7812.

Pennington, W. D., 1981. Subduction of the eastern Panama basin and seismotectonics of northwestern south America, *J. geophys. Res.,* **86,** 10753–10770.

Sieh, K. E., 1978. Slip along the San Andreas fault associated with the great 1857 earthquake, *Bull. seism. Soc. Am.,* **68,** 1421–1448.

Soulas, J. P., 1988. Tectonica activa y riesgo sismico, *Informe del Programma de prevencion y de planification para desastres en el Ecuador y Paises vecinos,* Proyecto UNDRO-EPN.

Soulas, J. P., Eguez, A., Yepes, H. & Perez, H., 1991. Tectonica activa y riesgo sismico, *Bol. Geol. Ecuat.,* Vol. 2, **1,** 3–11.

Stauder, W., 1975. Subduction of the Nazca plate under peru as evidence by focal mechanisms and by seismicity, *J. geophys. Res.,* **80,** 1053–1064.

Suarez, G., Molnar, P. & Burchfield, B. C., 1983. Seismicity, fault plane solutions, depth of faulting and active tectonics of the Andes of Peru, Ecuador and southern Colombia, *J. geophys. Res.,* **83,** 10403–10428.

Thouret, J.C., 1989. La Cordillère Centrale des Andes de Colombie et ses bordures–Morphogénèse liée au Plio–Quaternaire et dynamique actuelle et récente d'une cordillère volcanique englacée, *thèse de Doctorat,* Universite J. Fourier, Grenoble I.

Thouret, J.C. & Van Der Hammen, Th., 1981. Una secuencia holocenica y tardiglacial en la cordillera central de Colombia, *CIAF,* **6,** (1–3), 609–634.

Thouret, J.C., Van Der Hammen Th, Solomons, B. & Juvignes, E., 1993. Stratigraphy, chronology and palaeocology of the last glaciation in the Andean Central Cordillera, Colombia—A short note, *Z. Geomorph.* N.F., in press.

Van der Hammen, Th., 1981. The pleistocene changes of vegetation and climate in the Northern Andes, in *The glaciation of the Ecuadorian Andes,* pp. 125–145, ed. Hastenrath, S., A. A. Balkema, Rotterdam.

Winter, Th., 1990. Mécanismes des déformations récentes dans les Andes Equatoriennes, *thèse de Doctorat,* Université de Paris-Sud, Orsay.

Winter, Th. & Lavenu, A., 1989. Morphological and microtectonic evidence for a major active right-lateral strike–slip fault across central Ecuador (South America), *Ann. Tecton.,* **2,** 123–139.

Winter, Th, Iglesias, R. & Lavenu, A., 1989. Presencia de un sistema de fallas activas en el sur del Ecuador, *Biol. Geol. Ecuat.,* Vol. 1, **1,** 53–67.

Wright, H. E., 1984. Late glacial and Late Holocene moraines in the Cerros Cuchpanga, *Central Peru. Q. Res.,* **21,** 275–285.